PHILOSOPHICAL TRANSACTIONS OF THE ROYAL SOCIETY A MATHEMATICAL, PHYSICAL & ENGINEERING SCIENCES

The Adhesion of Thermoplastic Fibre Composites

A. J. Kinloch, G. K. A. Kodokian and J. F. Watts

Phil. Trans. R. Soc. Lond. A 1992 **338**, 83-112
doi: 10.1098/rsta.1992.0004

The adhesion of thermoplastic fibre composites

By A. J. Kinloch,[1] G. K. A. Kodokian[1]† and J. F. Watts[2]

[1] *Department of Mechanical Engineering, Imperial College of Science, Technology and Medicine, Exhibition Road, London SW7 2BX, U.K.*

[2] *Department of Materials Science and Engineering, University of Surrey, Guildford, Surrey GU2 5XH, U.K.*

Contents

† Present address: E.I. Du Pont, Experimental Station, Wilmington, Delaware 19880, U.S.A.

Phil. Trans. R. Soc. Lond. A (1992) **338**, 83–112
Printed in Great Britain

Fibre composites based upon thermoplastic polymeric matrices containing continuous fibres of carbon or 'Kevlar' are being increasingly used in engineering structures. Engineering applications frequently require that they be joined to components fabricated from similar fibre composites, or to other types of materials, and the use of structural adhesives, typically based upon epoxy resins, offers many advantages compared with other methods of joining. The present paper describes in detail the mechanics and mechanisms of the adhesion of thermoplastic fibre composites. The surface topography and chemistry of the composites have been characterized using contact angle measurements and X-ray photoelectron spectroscopy, both before and after using various surface treatments. Joints have then been prepared using epoxy adhesives and the adhesive fracture energies, G_c, of the joints have been measured. Two major aspects of the observed results, with wide applicability to many adhesion problems, have been analysed in detail. First, the need to apply a critical intensity of surface treatment to the thermoplastic fibre composite to prevent interfacial failure, and hence give relatively high values of G_c, has been interpreted by relating the chemical composition of the surface of the composite to the corresponding value of the polar force component of the surface free energy. It is thereby shown that the fundamental requirement is that a critical value of the surface polarity has to be attained. Secondly, after this critical value is reached, it is shown that the locus of joint failure may then be accurately predicted from a knowledge of the stress field in the joint and the experimentally measured interlaminar fracture stress of the fibre composite substrates.

1. Introduction

Polymer fibre composites based upon thermoplastic matrices, such as poly(aromatic amides) and poly(ether–ether ketone) and containing carbon or 'Kevlar' fibres, offer significant advantages compared with those based upon thermosetting polymeric matrices such as epoxy resins. For example, thermoplastic fibre composites may be readily thermoformed into components possessing a complex shape and usually exhibit a far higher interlaminar toughness (Leach *et al.* 1987). However, to realize the full advantages from thermoplastic fibre composites it is necessary to be able to join such composites to themselves, and to other materials.

One of the most widely used methods for joining the more conventional thermosetting polymer fibre composites is via the use of structural adhesives. This class of adhesives, typically based upon epoxy resins, possess a relatively high modulus and strength and are used to produce load-bearing joints. Now to obtain high strengths from joints which consist of thermosetting polymer fibre composites bonded using structural adhesives is a relatively straightforward task (see, for example, Kinloch 1987). Typically a simple abrasion treatment, followed by a solvent wipe to remove abraded debris, is sufficient to ensure that the locus of failure of the bonded joints is not at the adhesive/composite interface and that relatively tough and strong joints are formed.

PHILOSOPHICAL TRANSACTIONS OF THE ROYAL SOCIETY A MATHEMATICAL, PHYSICAL & ENGINEERING SCIENCES

However, Kinloch & Taig (1987) observed that obtaining high-strength joints when using the thermoplastic fibre composites was far more difficult. They found that a simple abrasion and solvent-wipe treatment was an inadequate surface treatment before bonding for these materials, since this form of treatment led to the joints failing at the adhesive/composite substrate interface at a relatively very low failure load. Later work by Kinloch & Kodokian (1988, 1989) demonstrated that a surface treatment based upon exposing the thermoplastic fibre composite to a 'corona discharge' was, however, particularly effective. Joints using such a surface treatment never failed at the adhesive/composite interface and possessed a high toughness and strength. Further, it was found that the problem of poor adhesion of structural adhesives to thermoplastic fibre composites appeared to be a general one; common, to a greater or lesser extent, to all such materials which were examined.

The present work reviews in detail the mechanics and mechanisms of the adhesion of thermoplastic fibre composites. The surface topography and chemistry of the composites have been characterized using contact angle measurements and X-ray photoelectron spectroscopy both before and after using various surface treatments. Joints have been prepared using two different epoxy adhesives, one which cures at room temperature and the other which cures at an elevated temperature. The adhesive fracture energies, G_c, of the joints have been ascertained using a linear-elastic fracture-mechanics approach, and the locus of joint failure has been identified.

It is found that after a certain, critical, intensity of corona treatment is used for the thermoplastic fibre composites the subsequently bonded joint no longer fails along the adhesive/composite interface. Instead, failure occurs either in the adhesive layer or in the fibre composite substrate, and this change in the locus of failure is associated with a far higher value G_c. Two major features of these observations, with wide applicability to many adhesion problems, have been analysed in detail. First, the need to apply a critical intensity of corona treatment to the surface of the thermoplastic fibre composite to prevent interfacial failure has been interpreted by relating the chemical composition of the surface of the composite to the corresponding polar force, γ_s^p, component of the surface free energy; the latter value being determined from contact angle measurements. It is thereby shown that the fundamental criterion for preventing interfacial failure is that a critical value of the surface polarity has to be attained. Secondly, after this critical value is reached, it is demonstrated that the locus of joint failure may then be accurately predicted from a knowledge of the stress field in the joint, found using finite element analysis methods, and the experimentally measured interlaminar fracture stress of the fibre composites.

2. The fibre composites and surface treatments

2.1. *The polymer fibre composites*

Nine different thermoplastic-based fibre composites, and one thermosetting-based composite, included for comparative purposes, were studied. These were the following.

(*a*) Unidirectional carbon-fibre/PEEK ('APC-2' composite from ICI plc). A continuous carbon-fibre composite containing a volume fraction of fibres of about 60% and a matrix of thermoplastic poly(ether–ether ketone) (termed u-carbon/PEEK in the present paper). The composite substrate was prepared by laying unidirectional tape into a 12-ply stack; the ply direction being $[0^0]_{12}$. As for all the

composite materials, sheets were prepared using a heated press. The temperature of the press was 380 °C and a pressure of 1.4 MPa was applied for 5 min.

(*b*) Unidirectional carbon-fibre/PA ('carbon-fibre/J2' composite from Du Pont, U.S.A.). A continuous carbon-fibre composite containing a volume fraction of fibres of 55 % and a matrix of a thermoplastic amorphous polyamide copolymer (termed u-carbon/PA). The polyamide is based on bis(para-aminocyclohexyl methane). The composite substrate was prepared by laying unidirectional tape into a twelve-ply stack; the ply direction being $[0^0]_{12}$. The temperature of the press was 300 °C and a pressure of 2 MPa was applied for 25 min.

(*c*) Woven carbon-fibre/PA ('woven carbon-fibre/J2' composite from Du Pont, U.S.A.). The same as in (*b*) except that the fibres were woven and the stack was made up of eleven plies (termed w-carbon/PA).

(*d*) Unidirectional 'Kevlar'-fibre/PA ('Kevlar-fibre/J2' composite from Du Pont, U.S.A.). A continuous Kevlar-fibre composite containing a volume fraction of fibres of 60 % and a matrix of a thermoplastic amorphous polyamide copolymer (termed u-Kevlar/PA). The composite substrate was prepared by laying unidirectional tape into a 16-ply stack; the ply direction being $[0^0]_{16}$. The temperature of the press was 300 °C and a pressure of 2 MPa was applied for 25 min.

(*e*) Woven Kevlar-fibre/PA ('woven Kevlar-fibre/J2' composite from Du Pont, U.S.A.). The same as in (*d*) except that the fibres were woven and the stack was made up of nine plies (termed w-Kevlar/PA).

(*f*) Woven carbon-fibre/PEI ('CYPAC X7005' composite from American Cyanamid, U.S.A.). A woven carbon-fibre composite containing a volume fraction of fibres of about 62 % and a matrix of thermoplastic poly(ether imide) (termed w-carbon/PEI). The composite substrate was prepared by laying the woven tape into an eight ply stack. The temperature of the press was 315 °C and a pressure of 0.7 MPa was applied for 30 min.

(*g*) Unidirectional carbon-fibre/PPS ('AC40–60' composite from Phillips Petroleum, U.S.A.). A continuous carbon-fibre composite containing a volume fraction of fibres of about 53 % and a matrix of thermoplastic poly(phenylene sulphide) (termed u-carbon/PPS). The composite substrate was prepared by laying unidirectional tape into a nine-ply stack; the ply direction being $[0^0]_9$. The temperature of the press was 360 °C and a pressure of 1.4 MPa was applied for 5 min.

(*h*) Unidirectional carbon-fibre/PI ('JD861' composite from British Petroleum plc). A continuous carbon-fibre composite containing a volume fraction of fibres of about 60 % and a matrix of a thermoplastic polyimide (termed u-carbon/PI). The composite substrate was prepared by laying unidirectional tape into a nine-ply stack; the ply direction being $[0^0]_9$. The temperature of the press was 300 °C and a pressure of 3.5 MPa was applied for 15 min.

(*i*) Woven carbon-fibre/PI ('JD861' composite from British Petroleum plc). The same as in (*h*) except that the fibres were woven and the stack was made of six plies (termed w-carbon/PI).

(*j*) Unidirectional carbon-fibre/epoxy ('913C XAS-5-34 %' composite from Ciba Geigy Ltd). A thermoset composite with a modified-epoxy resin matrix (termed u-carbon/epoxy). It was a continuous carbon-fibre composite containing a volume fraction of fibres of about 63 %. The composite substrate was prepared by laying unidirectional tape into a 12-ply stack, the ply direction being $[0^0]_{12}$. The temperature of the press was 150 °C and a pressure of 2 MPa was applied for 20 min. This thermoset composite was included for comparative purposes.

PHILOSOPHICAL TRANSACTIONS OF THE ROYAL SOCIETY A MATHEMATICAL, PHYSICAL & ENGINEERING SCIENCES

2.2. *Surface treatments*

Several different surface treatments were examined.

(*a*) Abrasion/solvent-cleaning. This is the typical treatment used for preparing composites based upon thermosetting polymeric matrices and the composite sheets were lightly abraded using 180/220 mesh alumina, then wiped clean with methyl–ethyl ketone and allowed to dry.

(*b*) Moulding next to clean aluminium foil. This method of preparing the thermoplastic fibre-composites was undertaken to ensure that no release agent was on the surface of the composite sheets. The aluminium foil was previously cleaned by etching the foil in a bath of chromic-acid solution to ensure that there were no release agents on its surface. After the moulding operation the aluminium foil was dissolved away from the surface of the thermoplastic composite sheet by using a bath of two molar sodium hydroxide solution.

(*c*) Corona discharge. This treatment involved exposing the thermoplastic composite sheets to an air plasma formed at atmospheric pressure. The major components of the corona discharge equipment were the generator producing high frequency (15–20 kHz) power (0.1–0.9 kW), the high-power transformer giving the high voltage (15–20 kV) and the high-power cables carrying the high voltage to the electrodes and the treater station. The equipment was designed to include two special features. First, conventional corona can readily treat non-conducting materials but the transformer of the present equipment was redesigned to give good impedance and capacitance matching between the electrode and the composite. For conducting materials a modified electrode was designed with a rubber silicone covering the surface, whereas for non-conducting materials a conventional knife-edged electrode was used. The second feature was that the power output from the electrode was current controlled, and not voltage controlled. Hence the power output from the electrode was directly obtained from the power gauge of the generator. After a light abrasion and a solvent wipe treatment, which is described above but which is not a critical requirement, the thermoplastic-composite substrates were placed on an automatically controlled table which travelled horizontally backwards and forwards under the discharge electrode. The velocity of the table could be selected as 14.5 mm s^{-1} to 62 mm s^{-1} and the velocity was controlled accurately by a stepper motor and a pulse generator (0.1–4.8 kHz). The energy output per unit area from the electrode onto the composites may be determined from

$$E = PN/LV, \tag{1}$$

where E is the energy output per unit area, P is the power of the high-frequency generator, N is the number of cycles of the table, L is the length of the treater and V is the velocity of the table.

3. Surface characterization

3.1. *Introduction*

The surfaces of the thermoplastic fibre composites were characterized before and after treatment using a variety of techniques. The surface topography was examined using scanning electron microscopy, the surface free energies of the composites were ascertained via the measurement of contact angles and the detailed chemical

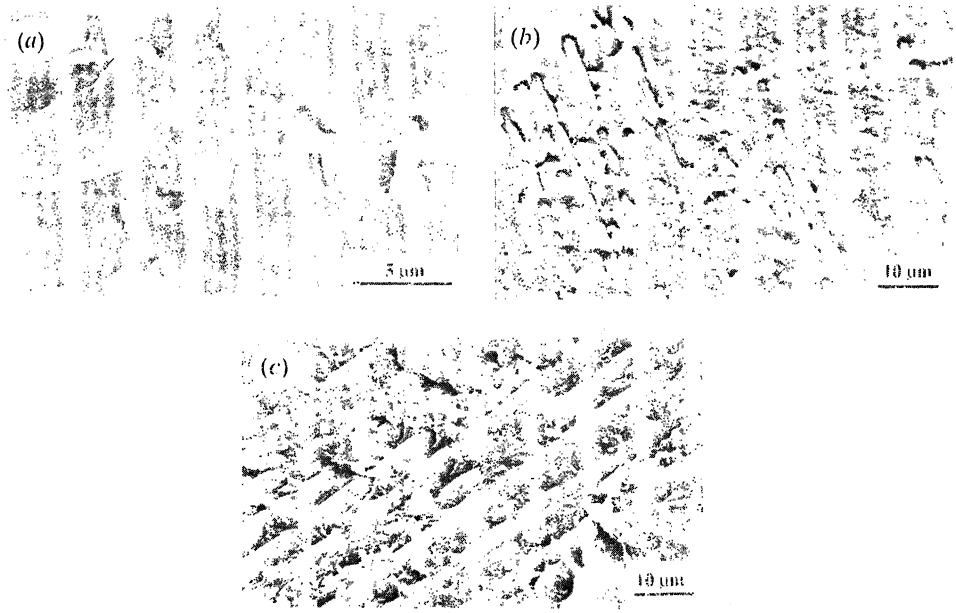

Figure 1. Scanning electron micrographs of unidirectional carbon-fibre/PEEK composite subjected to various treatments: (*a*) abrasion/solvent-wipe only; (*b*) corona treatment (20 J mm^{-2} of energy applied); (*c*) corona treatment (40 J mm^{-2} of energy applied).

compositions of the surface regions were identified using X-ray photoelectron spectroscopy.

3.2. *Surface topography*

The surface topography was studied using scanning electron microscopy. The surfaces of the fibre composite were first coated with a thin layer of gold to prevent charging of the specimen. In the case of the carbon-fibre based thermoplastic composites the effect of the corona treatment was to increase greatly the surface roughness of the composite, as may be seen from the micrographs shown in figure 1. Indeed, the micrographs shown in figure 1 reveal that corona treatment of the carbon/PEEK composite has resulted in ablation of the PEEK matrix to expose carbon fibres, and that these fibres have then been attacked by the corona discharge. For the carbon-fibre based composites such observations were typical for energy levels of corona treatment above about 20 J mm^{-2}. The degree of surface roughening was far less marked for the Kevlar fibre composites where ablation of the polymeric matrix to expose Kevlar fibres was never observed. These general observations applied to all the thermoplastic composites treated using a corona surface treatment. These differences in the behaviour of the composites based upon either carbon or Kevlar fibres are due to the former fibres being conductive, whereas the latter are non-conductive. The corona treatment involves a spark discharge which is attracted towards the conductive carbon-fibres and ablates the polymeric matrix covering the fibres.

3.3. *Surface free energy*

The surface free energies of the composite materials were determined from contact angle measurements. The various liquids used are shown in table 1 and also tabulated are the respective values of the dispersion force, γ_l^d, and polar force, γ_l^p, components

Table 1. *Surface free energies of liquids*

(Liquids supplied by the Dow Chemical Co. All data were taken from Fowkes (1967) and Dann (1970).)

liquids	surface free energy/(mJ m^{-2})		
	γ_l^d	γ_l^p	γ_l
water	22.0	50.2	72.6
glycerol	37.0	26.4	63.4
formamide	39.5	18.7	58.2
methylene iodide	48.6	0.0	48.6
1-bromonaphthalene	44.6	0.0	44.6
polyglycol E-200 *	28.2	15.3	43.5
dimethyl sulphoxide	29.6	13.7	43.3
iodoethanol	41.1	3.8	44.9

to the total surface free energy γ_l, of each liquid, where $\gamma_l = \gamma_l^d + \gamma_l^p$ (Fowkes 1967; Dann 1970). The advancing contact angle, α_r, was measured using the sessile drop method and sufficient time was allowed for equilibrium conditions to be reached. The average of at least six readings was taken and the reproducibility was within $\pm 3°$. However, two problems arose in obtaining values of γ_s^d and γ_s^p for the fibre composites from these measured contact angles. First, the corona surface treatment not only changed the surface chemistry but also changed the surface topography of the fibre composite. Both of these effects lead to a change in the measured contact angle and, hence, the surface free energy values. Secondly, existing methods of analysing the contact angle data were found to give relatively large scatter bands for the surface free energy values, and this hindered detailed interpretation of the results. These two problems were overcome as described below.

First, the fact that the surface treatment might affect both the surface chemistry and roughness of the composite was resolved by use of the Wenzel equation. Wenzel (1936) showed that the surface roughness alone may change the advancing contact angle, α_r, observed for a given liquid on a rough solid surface, compared with the angle, α_s, observed on a smooth surface of identical surface chemistry. This change in the contact angle may be expressed by

$$\cos \alpha_r = r_f \cos \alpha_s, \tag{2}$$

where r_f is the roughness factor, or the ratio of the actual area to the projection area of the solid. If the contact angle, α_s, on a smooth surface is less than 90°, then roughening will result in the contact angle, α_r, on the chemically equivalent but rougher surface, being even smaller. This will obviously increase the apparent surface free energy of the solid surface. However, if for a smooth surface α_s is greater than 90°, roughening the surface will increase the contact angle α_r still further, and therefore lead to a decrease in the apparent surface free energy.

Therefore, to allow for the changing surface roughness, all the fibre-composite surfaces of interest were coated with a thin layer of gold about 70 ± 5 nm in thickness, using a thermal evaporation coater, after the appropriate surface treatment had been conducted. Next, the contact angles of formamide and methylene iodide were measured on these gold-coated surfaces of (i) the untreated, (ii) the abraded/solvent-cleaned and (iii) the corona-treated fibre composites. A gold-coated glass microscope

Table 2. *Values of the surface roughness factor, r_f, for the unidirectional carbon-fibre/PEEK composite*

surface treatment	roughness factor, r_f
untreated	1.04 ± 0.02
abraded/solvent-wiped	1.09 ± 0.04
corona treated; intensity (J mm^{-2})	
0.25	1.10 ± 0.03
5.0	1.12 ± 0.03
10.0	1.13 ± 0.04
15.0	1.14 ± 0.04
20.0	1.18 ± 0.05
25.0	1.22 ± 0.05

slide was used as the reference (smooth) surface to obtain the value of α_s for each of the two liquids. Again, the average of at least six readings was taken and the reproducibility was within $\pm 3°$. The value of the roughness factor, r_f, was then deduced, using equation (2), for a given fibre composite which had been subjected to a given surface treatment. Typical values of the roughness factor, r_f, are given in table 2 for the carbon-fibre/PEEK composite. These values were not dependent upon the liquid used and the coefficient of variation was about $\pm 4\%$. As may be seen, the value of r_f increases with the severity of the surface treatment, confirming the increases in surface roughness which were observed from the scanning electron micrographs (see figure 1). Considering all the various fibre composites which were examined, the values of the roughness factor were typically in the range of 1.03 to 1.10 for the untreated composites, 1.09 to 1.15 for the abraded/solvent-wiped composites and 1.10 to 1.25 for the corona-treated composites. The next step was to allow for the effects of surface roughness on the measured values of the contact angle, α_r, using the appropriate value of r_f. Hence, the value of r_f for the composite surface of interest was used, together with the value of α_r for the given liquid/composite combination and equation (2), to deduce approximate values for the contact angle, α_s, for a smooth composite surface of the same surface chemistry. These values could now be used, as discussed below, to deduce the values of γ_s^d, γ_s^p and γ_s arising from changes solely in the surface chemistry of the composite.

Secondly, the values of the dispersion force, γ_s^d, and polar force, γ_s^p, components to the surface free energies of the composite materials have been previously evaluated using a derivation of the method originally proposed by Kaelble (1970). In the Kaelble analysis a pair of simultaneous equations is derived which for two liquids, i and j, on a common solid surface may be written as:

$$\left.\begin{aligned} 1+\cos\alpha_i &= \frac{2(\gamma_s^d)^{0.5}(\gamma_l^d)_i^{0.5}}{(\gamma_l)_i} + \frac{2(\gamma_s^p)^{0.5}(\gamma_l^p)_i^{0.5}}{(\gamma_l)_i} \\ 1+\cos\alpha_j &= \frac{2(\gamma_s^d)^{0.5}(\gamma_l^d)_j^{0.5}}{(\gamma_l)_j} + \frac{2(\gamma_s^p)^{0.5}(\gamma_l^p)_j^{0.5}}{(\gamma_l)_j} \end{aligned}\right\} \quad (3)$$

If the values of $\alpha, \gamma_l^d, \gamma_l^p$ and γ_l for the two liquids are known, these equations may be solved to yield the dispersion, γ_s^d, and the polar, γ_s^p, force components to the

Table 3. *Surface free energies of fibre composites subjected to an abrasion/solvent-cleaning surface treatment*

(For a full description of the fibre composites, see §2.1.)

fibre composite	surface free energy/(mJ m^{-2})		
	γ_s^d	γ_s^p	γ_s
u-carbon/epoxy	34.2±4.3	14.6±3.5	48.8±7.8
u-carbon/PEEK	39.5±2.2	2.9±0.8	42.2±3.0
u-carbon/PA	35.2±2.3	6.8±1.8	42.0±4.1
u-Kevlar/PA	34.8±3.2	7.5±1.9	42.3±5.1
w-carbon/PEI	35.7±2.9	5.0±1.4	40.7±4.3
w-carbon/PI	35.8±3.8	6.1±1.9	41.9±5.7
u-carbon/PPS	34.7±1.9	3.1±0.7	37.8±2.6

surface free energy of the solid surface. The total surface free energy, γ_s, is then simply the sum of these components. Thus, for each solid surface the values of γ_s^d, γ_s^p and γ_s may be evaluated from all dissimilar pair combinations of liquids by the use of equation (3). However, when using all the experimental data it was recognized (Kaelble 1970) that liquid pairs which contributed linear dependence in the simultaneous solution of equation (3) gave absurdly high values of γ_s^d and γ_s^p. Thus, inclusion of all the experimental data led to a very large scatter in the calculated values of γ_s^d and γ_s^p. From preliminary calculations it was considered that a suitable test condition was that, for inclusion, liquid pairs must possess an absolute value of $D \geqslant 10$ mJ m^{-2}, where

$$D = \{(\gamma_l^d)_i\,(\gamma_l^p)_j\}^{0.5} - \{(\gamma_l^d)_j\,(\gamma_l^p)_i\}^{0.5}. \tag{4}$$

However, whereas this led to a lower degree of scatter in the values of γ_s^d and γ_s^p so deduced, the scatter was still appreciable and the criterion for inclusion of the data given by equation (4) is obviously arbitrary. Therefore, a new method of analysing the contact angle data is proposed (see Appendix A) which is based upon a least squares method for solving equation (3). All the experimental data for the substrate surface of interest are included and the scatter associated with the values of γ_s^d and γ_s^p deduced from the analysis is relatively low. Therefore, a computer program was written to solve equation (A 7) and hence yield the values of γ_s^d and γ_s^p for the composite substrates. As discussed above, the values of the appropriate contact angles used in these calculations were taken to be the values after being corrected to allow for any changes in the surface roughness of the composite which accompanied changes in the surface chemistry.

The surface free energies of the various fibre-composite materials that have been subjected to a simple abrasion/solvent-cleaning treatment are shown in table 3. As may be seen, the thermosetting epoxy-based composite possesses a relatively high surface free energy, γ_s, and the polar force component, γ_s^p, makes a very significant contribution to the value of γ_s. For the thermoplastic fibre composites the values of γ_s^d are somewhat similar in value to each other, and to the value of γ_s^d for the thermosetting fibre composite. However, considering the polar force, γ_s^p, component, then the exact value of γ_s^p for a thermoplastic fibre composite is dependent upon the chemical type of the matrix present, but in all cases the value of γ_s^p for the thermoplastic fibre composites is significantly lower than that for the thermosetting fibre composite.

PHILOSOPHICAL TRANSACTIONS OF THE ROYAL SOCIETY A MATHEMATICAL, PHYSICAL & ENGINEERING SCIENCES

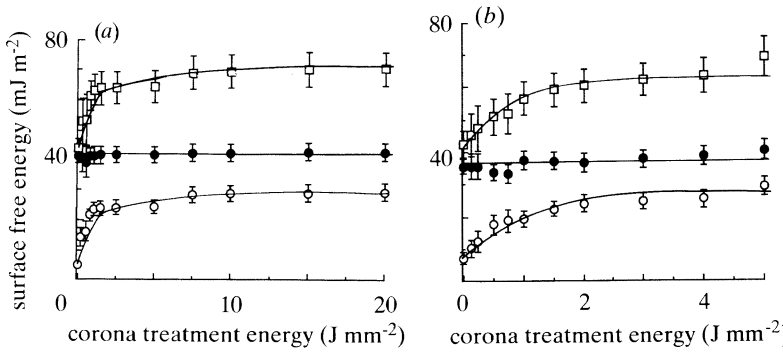

Figure 2. Surface free energy against level of corona treatment energy applied. (*a*) Unidirectional carbon-fibre/PEEK composite; (*b*) unidirectional carbon-fibre/PA composite. □, total (γ_s); ●, dispersion (γ_s^d); ○, polar (γ_s^p).

The typical effect of corona treatment on values of γ_s^d, γ_s^p, and γ_s for two of the thermoplastic fibre-composites studied is illustrated in figure 2. As the level of corona treatment is increased the surface free energy increases up to a maximum plateau value, and this arises from the value of γ_s^p increasing as the level of the corona treatment energy is increased. Indeed, the value of γ_s^d is independent of the level of corona treatment employed. The exact form of the relation between γ_s^p and the corona treatment level was dependent upon the chemical type of matrix used, but the data in figure 2 are representative of all the thermoplastic fibre composites examined.

Finally, it should be noted that other relations, besides the geometric mean given above in equation (3), have been suggested to obtain the values of γ_s^d and γ_s^p from contact angle data; for example the reciprocal mean (Wu 1971) and harmonic mean (Wu 1973) have also been proposed. However, the concept of using the geometric mean has received both theoretical (Good 1971; Barton 1982) and experimental support (Schultz *et al.* 1977; Baszkin *et al.* 1977) and will therefore be used in the present studies. Indeed, when the contact angle measurements reported in Appendix A were analysed using the reciprocal mean approach the values of γ_s^d and γ_s^p so obtained were clearly a function of the actual liquid pair which was selected and no sensible average values could be ascertained.

3.4. *Chemical composition of the surface regions*

The detailed surface chemistry of the fibre composites was studied using X-ray photoelectron spectroscopy (XPS). A VG Scientific ESCALAB Mk II system equipped with a VGS-5000S data system was used and AlKα radiation was used for all analyses. Peak fitting of the carbon (C1s) spectra into its individual components was achieved using an iterative least squares fitting routine. The full details of the surface analyses have been previously reported by Kodokian (1990).

The surface analyses of the fibre composites which have been subjected to solely an abrasion/solvent-cleaning treatment are shown in table 4. Comparing these data with those for the as-received (i.e. untreated) composites reveals that the abrasion/solvent-cleaning treatment has reduced the silicon and fluorine contamination from levels of typically about 3 to 4 at.% for the untreated composites to concentrations of about 1 to 2 at.%. This contamination is undoubtedly

PHILOSOPHICAL TRANSACTIONS OF THE ROYAL SOCIETY A MATHEMATICAL, PHYSICAL & ENGINEERING SCIENCES

Table 4. *Atomic % concentrations of elements detected (using* XPS*) on the surfaces of the fibre composites subjected to an abrasion/solvent-cleaning surface treatment*

fibre composite	C1s	O1s	N1s	Si2p + F1s	S2p	Na1s
u-carbon/epoxy	81.0 ± 2.2	15.7 ± 0.9	1.7 ± 0.5	1.1 ± 0.5	nd	nd
u-carbon/PEEK	77.6 ± 1.5	18.1 ± 1.1	0.4 ± 0.4	2.2 ± 0.5	nd	nd
u-carbon/PA	75.9 ± 1.8	18.1 ± 0.9	3.8 ± 0.8	1.2 ± 0.4	nd	1.1 ± 0.5
u-Kevlar/PA	73.1 ± 1.7	18.3 ± 1.0	4.0 ± 0.8	1.6 ± 0.3	nd	nd
w-carbon/PEI	71.8 ± 2.1	22.7 ± 0.8	3.7 ± 0.9	1.0 ± 0.4	nd	0.7 ± 0.5
w-carbon/PI	69.8 ± 1.9	23.5 ± 1.3	3.4 ± 0.9	1.3 ± 0.4	nd	1.3 ± 0.4
u-carbon/PPS	82.3 ± 1.7	7.3 ± 0.7	1.2 ± 0.3	1.7 ± 0.5	7.2 ± 0.7	nd

nd: not detected.

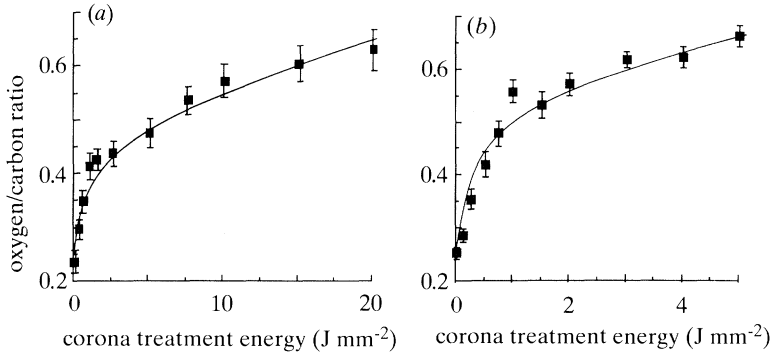

Figure 3. Oxygen : carbon ratio determined from XPS analysis against intensity of corona treatment energy applied. (*a*) Unidirectional carbon-fibre/PEEK composite; (*b*) unidirectional carbon-fibre/PA composite.

associated with the release agents which were used to coat the mould. This is confirmed by the results on the carbon/PEEK thermoplastic composite which had been moulded against clean aluminium foil, which was subsequently dissolved away. The surface of this composite possessed no detectable concentrations of silicon or fluorine contamination.

XPS analysis of the thermoplastic fibre composites after corona treatment revealed several major changes to the surface composition, which were observed for all the various types of thermoplastic fibre composites studied. First, the oxygen : carbon elemental ratio increases as the level of corona treatment is increased. This is clearly illustrated in figure 3. Secondly, further details of the chemical changes which accompany this increased concentration of oxygen in the surface regions of the composites were obtained by deconvolution of the narrow XPS scan of the carbon peak. Typical results of such an analysis for the unidirectional carbon-fibre/PA composite are given in figure 4 and more detailed results are given in table 5 for the woven carbon-fibre/PI composite. It may be seen that the corona treatment has led to a dramatic increase in the concentration of oxygenated species, as noted above. In particular, there is an increase in the concentration of carbonyl (C=O) groups and the introduction of carboxylic acid (O–C=O) groups. Thirdly, it was also found that for all the thermoplastic fibre composites that the level of the nitrogen elemental

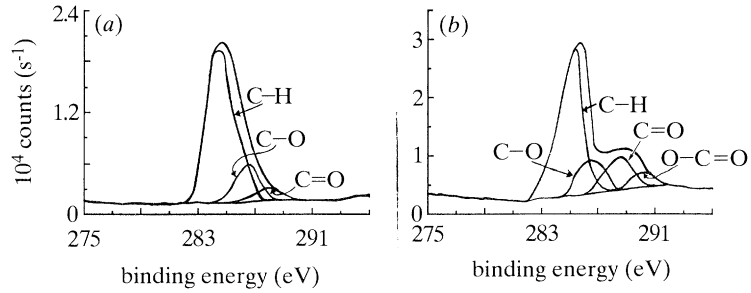

Figure 4. Narrow XPS scans of the carbon 1s peak of the unidirectional carbon-fibre/PA composite. (*a*) Abraded/solvent-wiped only; (*b*) corona treatment (5 J mm^{-2} of energy applied).

Table 5. *Atomic % concentrations of groups present in the C1s XPS peak for the woven carbon-fibre/polyimide composite as a function of the intensity of the corona treatment*

corona treatment intensity (J mm^{-2})	C–H	C–O	C=O	O–C=O
0	82.0±1.0	14.0±1.0	4.0±1.0	nd
0.25	79.5±1.5	15.5±0.5	5.0±1.0	nd
0.50	77.0±1.0	16.0±1.0	6.0±1.0	1.0±1.0
0.75	75.5±1.5	16.5±0.5	7.0±1.0	1.0±1.0
1.00	75.0±0.0	16.0±1.0	8.0±1.0	1.5±0
2.00	72.0±1.0	16.0±1.0	10.0±0.5	2.0±0
3.00	70.0±2.0	16.5±1.0	10.5±0.5	2.5±0
4.00	70.5±0.5	14.0±1.0	12.0±1.0	3.0±0

nd: not detected.

peak increased considerably as the intensity of corona treatment was increased. Analysis of the binding energy revealed that the nitrogen had not combined with oxygen, but with carbon to possibly form amine groups. Fourthly, except for the Kevlar fibre composites, the concentration of silicon and fluorine decreased as the level of corona treatment was increased. The concentration fell steadily from the values of about 1 to 2 at.% shown in table 4 for the composites before corona treatment to a minimum of about 0.5 to 0.75 at.%. In the case of the Kevlar fibre composites little change was observed after corona treatment, so the concentration remained at about 1.6 at.%. These observations can be directly correlated to the results from the scanning electron microscopy studies. This work revealed that, unlike the carbon-fibre composites, the Kevlar fibre composites did not suffer from ablation of the matrix during the corona treatment. Removal of the matrix would obviously be an effective means of removing relatively low concentrations of silicon and fluorine based contamination from the surfaces of the composites. Finally, in the case of the carbon-fibre/poly(phenylene sulphide) composite, the corona treatment also led to the introduction of S=O groups, which increased in concentration as the level of corona treatment increased.

In an attempt to estimate the depth of the surface regions which had been affected by the corona treatment the XPS analysis of the C1s peak was repeated using various take-off angles for the emitted photoelectrons. The data reported above were for a

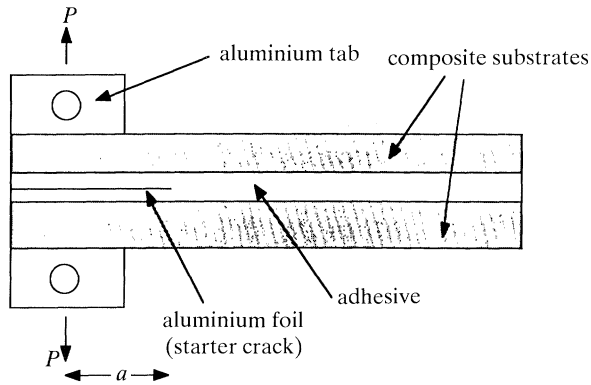

Figure 5. The double-cantilever beam (DCB) joint specimen.

take-off angle of 45° and this angle was now varied from 15° through to 90°. Assuming an inelastic mean free path of 2.3 nm for C1s (Cave *et al.* 1990) the equivalent depths of analysis were 1.8 nm to 6.9 nm. However, the XPS spectra for the fibre composites showed no significant change in either the intensity or the shape of the C1s peak. This demonstrates that the surface regions are uniformly affected to a depth of greater than about 7 nm by the corona treatment.

4. The adhesive fracture energy

4.1. *Preparation of adhesive joints*

The toughness of adhesive joints prepared using the polymer fibre composites as the substrate materials was assessed by using a continuum fracture mechanics analysis to ascertain the adhesive fracture energy, G_c. Double cantilever beam (DCB) joints were prepared as illustrated in figure 5. The substrates were cut from the laminate sheet, of thickness 1.5 mm, and were 20 mm wide. The adhesive used was either a two-part cold-cured epoxy paste adhesive ('EA 9309' from Hysol Dexter, U.S.A.) or a one-part hot-cured epoxy film adhesive ('FM73M' from American Cyanamid, U.S.A.). The initial starter crack was made by inserting a release-coated aluminium foil in between the adhesive-coated composite substrates. To effect cure of the adhesive, the joints prepared using the two-part cold-cured epoxy-paste adhesive were kept at 21 ± 2 °C under a pressure of 69 kPa, whereas those using one-part hot-cured epoxy film adhesive were kept at 120 °C for one hour under a pressure of 275 kPa. The test specimen was completed by bonding on to each side of the DCB joint the metal end blocks, using a room-temperature curing adhesive. The edges of the DCB specimens were painted white using a typewriter correction fluid and were marked off at 5 mm intervals along the complete length of the beam.

The DCB joints were mounted in a screw-driven tensile testing machine and loaded under displacement control at a crosshead speed of 2 mm min^{-1}. The load against displacement trace for the specimen was monitored, and linear-elastic behaviour was always recorded. The crack was monitored using a travelling microscope mounted on a stand and, as the crack propagated and crossed the markers, a mark was made on the associated load against displacement trace. The adhesive fracture energy, G_c, was

Table 6. *Joint and composite failure properties*

	adhesive				composite
	cold-cured epoxy		hot-cured epoxy		properties
composite	G_c (plateau)	L of F	G_c (plateau)	L of F	G_c (il)
u-carbon/epoxy	0.25	il	1.90	coh	0.25
u-carbon/PEEK	3.90	coh	1.86	coh	2.30
u-carbon/PA	3.78	coh	1.79	coh	1.10
w-carbon/PA	3.84	coh	1.84	coh	1.15
u-Kevlar/PA	0.64	il	0.66	il	0.65
w-Kevlar/PA	0.71	il	0.70	il	0.68
u-carbon/PI	1.51	il	1.50	il	1.46
w-carbon/PI	1.69	il	1.86	coh	1.68
w-carbon/PEI	1.67	il	1.84	coh	1.60
u-carbon/PPS	1.47	il	1.47	il	1.45

Notes.

(i) G_c (plateau): the plateau value of the adhesive fracture energy. For the thermoplastic composites this occurs after a given intensity of corona treatment has been applied to the composite prior to bonding. Obviously, for the carbon-fibre/epoxy composite this is simply the measured value after an abrasion/solvent-wipe surface treatment, since no corona treatment is needed for this composite to prevent interfacial failure occurring.

(ii) 'G_c(il)': the interlaminar fracture energy for the composite.

(iii) All G_c values are in kJ m^{-2}.

(iv) 'L of F': locus of joint failure; 'coh': cohesive in adhesive layer failure; 'il': interlaminar fracture in composite substrate.

determined using the following relation, which is based upon a standard linear-elastic fracture-mechanics analysis (Irwin 1964):

$$G_c = (P_c^2 \, \mathrm{d}C/2B) \, \mathrm{d}a \tag{5}$$

and

$$C = \Delta/P, \tag{6}$$

where P_c is the load for crack growth, P is the load, B is the width, a is the crack length, Δ is the displacement and C is the compliance of the specimen. All these parameters were directly determined and the partial derivative of the compliance with crack length was evaluated by writing a simple computer programme to curve-fit the experimental data of the compliance against the crack length.

4.2. G_c *values from using abraded/solvent-cleaned composite substrates*

The values of the adhesive fracture energy, G_c, and the locus of joint failure for the DCB joints prepared using the thermosetting polymer-fibre composite, which was the unidirectional carbon-fibre epoxy composite, are given in table 6. As may be seen, the value of G_c when using the hot-cured epoxy adhesive is 1.9 kJ m^{-2} but is only 0.25 kJ m^{-2} when using the cold-cured epoxy adhesive. The reason for the relatively low G_c value in the latter case may be readily understood from the observation that the locus of joint failure when using the former, hot-cured, adhesive is via cohesive fracture through the adhesive layer, but for the latter joints is via interlaminar fracture through the epoxy-based fibre composite; i.e. when using the cold-cured adhesive the joint fails by a new crack initiating and propagating between the

PHILOSOPHICAL TRANSACTIONS OF THE ROYAL SOCIETY A MATHEMATICAL, PHYSICAL & ENGINEERING SCIENCES

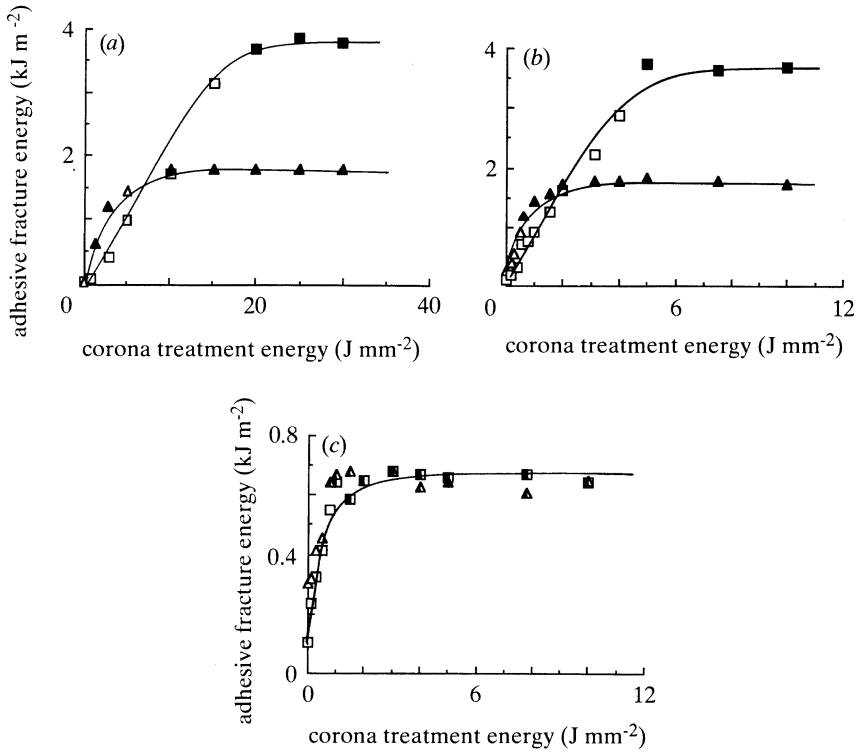

Figure 6. The adhesive fracture energy, G_c, against the intensity of corona treatment for the thermoplastic fibre-composite. (*a*) Unidirectional carbon-fibre/PEEK composite; (*b*) unidirectional carbon-fibre/PA composite; (*c*) unidirectional Kevlar-fibre/PA composite. □, cold-cured epoxy adhesive (interfacial failure); ■, cold-cured epoxy adhesive (cohesive failure in adhesive layer); △, hot-cured epoxy adhesive (interfacial failure); ▲, hot-cured epoxy adhesive (cohesive failure in adhesive layer); ◭, ◧, interlaminar failure in the composite substrate.

laminae forming the composite substrate. The reasons for these different failure modes are discussed later, but for the present it should be noted that no interfacial failure was ever observed in these joints. Thus, in accord with previous work, the light abrasion/solvent-wipe treatment that this thermosetting-based composite received before bonding was sufficient to ensure adequate intrinsic adhesion at the adhesive/composite substrate interface.

However, a very different picture emerges when the thermoplastic fibre composites, which have been simply abraded and solvent-cleaned, are considered. In all cases the values of G_c determined for the DCB joints were very low, typically about 0.02 to 0.03 kJ m^{-2}, and the locus of joint failure appeared, from a visual assessment, at the adhesive/composite interface. These data clearly establish the need to use a more effective surface treatment for the thermoplastic fibre composites which will ensure adequate intrinsic adhesion of the thermoplastic fibre composite to the epoxy adhesives.

4.3. *G_c values from using corona-treated thermoplastic fibre composite substrates*

The effect of using a corona treatment for the thermoplastic-fibre composites before adhesive bonding is illustrated in figure 6, where it may be seen that this

treatment has led to dramatic increases in the values of G_c for a range of different types of thermoplastic fibre composites. However, two different patterns of behaviour emerge from the results shown in figure 6. Firstly, the data in figure 6*a* and 6*b* for the carbon-fibre/PEEK and carbon-fibre/PA composites bonded with either the cold-cured or hot-cured adhesive are very similar in form. Namely, the value of G_c rises to a maximum, plateau, value as the intensity of corona treatment used before bonding is increased. This is accompanied by a change in the locus of failure from apparently interfacial to cohesive in the adhesive layer. (It is noteworthy that one significant difference in figure 6*a* and 6*b* is that the intensity of corona treatment needed to attain the plateau value of G_c is significantly less for the carbon-fibre/PA composite than that required for the PEEK composite. The reasons for this observation are discussed in detail later when the fracture behaviour and the surface chemistry results are correlated.) Secondly, however, for the unidirectional Kevlar-fibre/PA composite bonded with either adhesive the data in figure 6*c* reveals that, whereas the corona treatment has increased the value of G_c, the plateau values are only about 0.65 kJ m^{-2}. This value may be compared with the plateau values of about 3.9 kJ m^{-2} and 1.9 kJ m^{-2} for the cold-cured and hot-cured adhesives respectively when bonding the corona-treated carbon-fibre/PEEK (figure 6*a*) and carbon-fibre/PA (figure 6*b*) composites. The reason for these lower values of G_c (plateau) for the bonded Kevlar-fibre/PA composites is evident from the data given in table 6, where it is shown that the locus of joint failure was via interlaminar fracture through the composite substrates. Thus, whereas the corona treatment has been effective in preventing interfacial failure along the adhesive/composite interface, the 'weak link' in the joint is now the premature delamination of the composite substrate itself, and the value of G_c (plateau) is very similar to that of the interlaminar fracture energy, G_c(il), of the composite material.

The plateau values of G_c, and associated loci of joint failure, for the DCB joints for all the bonded composite joints studied are given in table 6 and, as may be seen, the values of G_c (plateau) and loci of failure are dependent upon the type of composite and adhesive used. Nevertheless, it should be noted that for all the thermoplastic fibre composites the use of the corona treatment before bonding prevents interfacial failure occurring.

4.4. *Bulk fracture behaviour of the adhesives*

Finally, it is of interest to note that the bulk fracture behaviour of the adhesives was also studied. It was not possible to prepare bulk test specimens from the hot-cured epoxy adhesive, since it is in the form of a thin film. However, single-edge notched three-point-bend samples were prepared using the cold-cured epoxy-paste adhesive and the value of the fracture energy, G_{1c}, for crack initiation was measured (Kodokian 1990). The value of G_{1c} for this adhesive was found to be 3.9 kJ m^{-2}. This value is in excellent agreement with that determined from the adhesive joints prepared using this adhesive when the locus of joint failure was cohesive failure through the adhesive layer. The results from these studies thus emphasize the intriguing observations, shown in table 6, where the value of G_c (plateau) for the joints can exceed the interlaminar fracture energy of the composite being bonded. These observations are discussed in detail below.

5. Locus of joint failure

5.1. *Introduction*

The above studies have clearly shown that for the thermosetting epoxy fibre composite a simple abrasion/solvent-wipe treatment for the composite before adhesive bonding is all that is needed to ensure a sufficiently good interfacial strength to prevent joint failure occurring at the adhesive/composite interface. The bonded DCB joints then fail by interlaminar failure of the composite substrate or by cohesive fracture through the adhesive layer, depending upon the adhesive being used. However, in the case of the thermoplastic composites a corona pretreatment is necessary to prevent the adhesive/composite interface failing at a very low value of G_c, and after treatment to a given intensity of corona energy the value of G_c reaches a maximum, plateau value. In some cases this does correspond to a cohesive fracture through the adhesive layer at a high value of G_c. However, in other cases the 'weak link' now appears to be the composite substrate itself. In these instances a new crack initiates very close to the adhesive/composite interface and just above and/or below the starter crack placed in the adhesive layer. This interlaminar crack then propagates through the composite substrate resulting in joint fracture.

The above points may be clearly seen from the data shown in table 6. First, note that when the bonded joint fails by interlaminar fracture of the composite substrate the associated value of the maximum adhesive fracture energy, G_c (plateau), attained is significantly lower than when the locus of joint failure is via cohesive fracture through the adhesive layer. Indeed, when the joints fail by interlaminar fracture of the composite the measured value of G_c is very similar to that of the interlaminar fracture energy, G_c(il), as would be expected. The important practical consideration is that such an interlaminar crack propagates at an applied load, and hence an adhesive fracture energy, G_c, below that associated with cohesive failure through the adhesive layer. Secondly, there is a greater tendency for the joints using the cold-cured epoxy adhesive to exhibit an interlaminar failure of the composite substrate. This arises from the cold-cured adhesive being the far tougher of the two epoxy adhesives used and, hence, higher loads need to be applied to the joint to cause crack growth through the adhesive layer. These higher loads will give rise to higher stresses in the composite substrate. Therefore, whereas the composite substrates may be able to withstand delamination when bonded with the less tough hot-cured epoxy adhesive, they tend to delaminate when subjected to the higher loads and stresses which can be imposed when the tougher cold-cured adhesive is used. Thirdly, there appears to be little correlation between the interlaminar fracture energy, G_c(il), of the composite and the propensity of the adhesive joint to fail by interlaminar failure of the composite substrate. For example, the epoxy-based composite has by far the lowest G_c(il) value, but when bonded using the hot-cured adhesive the joints show no signs of any interlaminar failure. Similarly, note that the unidirectional and the woven carbon-fibre/PA thermoplastic composites possess only moderate values of G_c(il), but again the DCB joints using these composites show no signs of any interlaminar fracture. Alternatively, the carbon-fibre/PPS composite possesses a relatively high interlaminar toughness, but the DCB joints always fail by delamination of the composite substrate. Thus, somewhat surprisingly, it appears that some property other than the interlaminar toughness of the composite must control its tendency to delaminate.

PHILOSOPHICAL TRANSACTIONS OF THE ROYAL SOCIETY A MATHEMATICAL, PHYSICAL & ENGINEERING SCIENCES

Table 7. *Values of the calculated out-of-plane transverse stresses, σ_{yy} (from FEA), compared with the measured transverse fracture stresses, σ_{yyc}, for the composite materials*

(All figures are in MPa. Abbreviations as table 6.)

	adhesive				
	cold-cured epoxy		hot-cured epoxy		composite material
composite	σ_{yy}	L of F	σ_{yy}	L of F	σ_{yyc}
u-carbon/epoxy	82.0	il	55.9	coh	58.9
u-carbon/PEEK	81.9	coh	55.8	coh	84.3
u-carbon/PA	81.9	coh	55.9	coh	83.7
w-carbon/PA	79.1	coh	54.2	coh	83.7
u-Kevlar/PA	71.4	il	48.8	il	21.5
w-Kevlar/PA	81.1	il	54.5	il	21.5
w-carbon/PI	76.5	il	54.6	coh	56.1
u-carbon/PPS	82.0	il	56.1	il	29.4

5.2. *Stress analysis*

The studies described above revealed that any new interlaminar crack that developed did so in the immediate vicinity of the crack which was initially inserted in the adhesive layer. The stress field surrounding the crack in the adhesive layer will extend into those regions of the composite substrates above and below the crack tip in the adhesive layer and will give rise to out-of-plane tensile stresses, σ_{yy}. These stresses will act to delaminate the composite substrates. Thus, to predict quantitatively the tendency of the composite substrate to initiate an interlaminar crack, it is necessary to compare the value of σ_{yy} for a given joint with the out-of-plane transverse tensile fracture stress, σ_{yyc}, of the composite materials which form the substrates. To ascertain the values of the out-of-plane transverse tensile stresses a numerical finite element analysis (FEA) approach was adopted, and this is described in Appendix B. The out-of-plane transverse tensile fracture stresses of the composite materials used in the present studies were experimentally measured (ASTM 1977).

5.3. *Criterion for determining the locus of joint failure*

The values of the out-of-plane transverse tensile stresses in the composite substrates are given in table 7 for the various adhesive/composite joints. These values of σ_{yy} have been calculated using the value of the applied load for the DCB joint that would be necessary to cause a cohesive fracture through the adhesive layer. The location of these predicted out-of-plane transverse stresses listed in table 7 is just inside the composite substrate, above and below the crack tip (see Appendix B, figure 10). Also, given in this table are the experimentally measured out-of-plane transverse tensile fracture stresses for the composite materials. Now, for those cases when the calculated values of σ_{yy} are lower than the measured out-of-plane transverse tensile fracture stress of the composite, it would be predicted that interlaminar fracture of the composite would not occur. Thus, the DCB joint would be expected to fail by the crack growing cohesively through the adhesive layer. Conversely, when the calculated values of σ_{yy} are higher than the measured out-of-plane transverse tensile fracture stress of the composite, then it would be predicted that delamination of the composite substrate would now be the preferred mode of failure.

As may be seen from the data presented in table 7, the predictions based upon the above arguments are in excellent agreement with the experimental observations of the locus of joint failure. Thus, the locus of joint failure for DCB joints is governed by the value of the transverse tensile stress generated in the composite substrate in the region of the crack tip, relative to the transverse fracture stress of the composite; assuming that a sufficiently adequate surface treatment, to ensure good intrinsic adhesion across the adhesive/composite interface, has been used for the composite substrate before bonding. The locus of joint failure is, therefore, governed by the ease of initiating an interlaminar crack in the composite substrates, rather than the energy needed to subsequently propagate this interlaminar crack through the composite substrate. The initiation process is controlled by the magnitude of the local stress field and the transverse fracture strength of the composite material.

6. Adhesion mechanisms

6.1. *Introduction*

It has been described above how a wide range of thermoplastic fibre composites may be successfully bonded using epoxy-based structural adhesives, if the composites are subjected to a corona surface treatment before adhesive bonding. The surface free energies and chemical compositions of the surfaces of the composites have been analysed and the fracture energies of the bonded joints have been measured. The discussions below consider the quantitative correlation of these data.

6.2. *Weak boundary layers*

The role of weak boundary layers in influencing the strength and toughness of adhesive joints has been extremely controversial. Some workers (see, for example, Bikerman 1968) believe that they are omnipresent, whereas others (see, for example, Kinloch 1987; Briggs *et al.* 1976) consider that their role in influencing the failure of adhesive joints is more limited.

The first, and most obvious, type of weak boundary layer to consider is the presence of residual mold release agents, based upon fluorine and silicon compounds of low-molecular weight and which are used in the manufacture of the composite sheets. The presence of such release agents could clearly be very detrimental to the attainment of high joint strengths. Now, after an abrasion/solvent-cleaning treatment the concentration of silicon and fluorine elements on the composite surfaces is similar for both the thermosetting and the thermoplastic composites, as may be seen from table 4; and this relatively low level of surface contamination does not hinder the development of high joint strengths for the epoxy composites. Further, when the carbon-fibre/PEEK thermoplastic composite was molded against clean aluminium foil, and the foil subsequently removed by etching in a sodium hydroxide solution, there was no detectable level of silicon or fluorine on the surface of the composite. Nevertheless, the bonded joints still showed failure at the adhesive/composite interface at a very low value of G_c. So clearly, simply removing the low level of residual contamination from the surface of the thermoplastic composites before bonding is insufficient to ensure good joint strengths.

A second type of weak boundary layer described in the literature is where the surface regions of the substrate possess an inherent weakness, and joint failure occurs through the surface regions of the substrate, close to the interface (Bikerman 1968; Kinloch & Yuen 1989). To examine this possible mechanism the fracture surfaces of

PHILOSOPHICAL TRANSACTIONS OF THE ROYAL SOCIETY A MATHEMATICAL, PHYSICAL & ENGINEERING SCIENCES

Table 8. *XPS analysis of the fracture surfaces of a joint consisting of carbon-fibre/PEEK substrates bonded using the cold-cured epoxy adhesive*

(The composites were abraded/solvent-cleaned only. The 'adhesive control' surface was formed by the cohesive fracture of a specimen of the adhesive.)

surface	atomic % concentrations of elements		O1s:C1s ratio
	C1s	O1s	
composite substrate before bonding	77.6±1.5	18.1±1.1	0.23
adhesive control	88.4±1.7	7.8±0.8	0.09
composite substrate from failed joint	78.6±1.7	17.1±0.7	0.22
adhesive from failed joint	87.6±1.8	8.0±0.7	0.09

a joint consisting of carbon-fibre/PEEK composite substrates, which had been simply abraded/solvent-cleaned and then bonded using the cold-cured epoxy adhesive, were analysed. Optical and electron micrographs of the fracture surfaces revealed that apparent interfacial failure had occurred. However, to ensure that joint failure had not occurred in a layer very close to the interface, which was too thin to be detected using the microscopy techniques, XPS analyses of the fracture surfaces were also undertaken. These results are shown in table 8. First, it is noteworthy that the O1s:C1s ratio for the surfaces of the composite substrate before bonding and the adhesive control are significantly different to one another. Thus, by comparison of these ratios to those from the fracture surfaces of a failed joint, the locus of joint failure may be identified. Secondly, the ratio for the composite substrate from the failed joint is identical to that found for the composite before being bonded, and a similar picture emerges for the adhesive surfaces. These observations confirm the results from the microscopy studies and demonstrate that the failure in these joints is truly at the adhesive/composite interface.

Thus, there is no evidence that any type of weak boundary layer plays a role in the failure of the thermoplastic composite/adhesive joints.

6.3. *The effect of surface topography*

The scanning electron micrographs of the thermoplastic fibre composites shown in figure 1 clearly revealed that the surface roughness increased after corona treatment. However, it was found that this increase in surface roughness could be prevented by using a relatively thick layer of matrix on the outermost surface of the fibre-composite. Therefore, to eliminate the possibility that the increase in surface roughness allowed some form of mechanical interlocking to occur between the adhesive and the composite substrate, unidirectional carbon-fibre/PEEK and unidirectional carbon-fibre/PA composite sheets were prepared with a relatively thick layer of about 500 μm of the thermoplastic matrix on their outermost surfaces. These composites were then treated using the corona treatment and electron microscopy studies and XPS analyses were conducted. The results (Kodokian 1990) revealed that the use of the relatively thick layer of matrix led to only very small changes in the surface roughness and that the surface chemical composition of the composite was not significantly different to that for the composites where the usual thin layer of matrix was present, when comparisons were made at the same intensity

Table 9. *Dipole moments for some chemical bonds*

chemical bond	dipole moment/Debye
C–N	0.2
C–O	0.7
C═O	2.3
O–C═O	2.0
S═O	2.3
N–H	1.3

of corona treatment. When DCB joints were made and tested it was found that the values of the adhesive fracture energies, G_c, were not dependent upon whether a thin or thick layer was present on the outermost surfaces of the composites. Thus, there is no evidence that the degree of surface roughness has any major effect on the intrinsic adhesion at the adhesive/composite interface.

6.4. *Relations between the surface chemistry of the fibre composites and the adhesive fracture energies*

The conclusions from the above studies emphasize the importance of the changes in the surface chemistry of the thermoplastic fibre-composites which result from using the corona treatment. It has been shown that an increase in the surface concentration of polar groups, such as oxygen-containing groups, leads to an increase in the surface free energy of the fibre-composite substrate. This will lead to an increase in both the extent of wetting by the epoxy adhesive on the substrate and in the intrinsic adhesion across the adhesive/composite interface. These effects will result from enhanced interfacial interactions arising from dipole-induced dipole, dipole–dipole, hydrogen bonds and acid–base forces. This enhancement in intrinsic adhesion is reflected in the locus of failure of the DCB joints no longer being at the adhesive/composite interface, and the far higher values of G_c which are now recorded.

The increases in surface polarity from using the corona pretreatment are obviously reflected in both the measured polar force component, γ_s^p, and the increased oxidation of the surface regions of the thermoplastic fibre composite which is evident from the XPS studies. The polar surface forces, which are reflected in the value of γ_s^p, arise from the orientation of electric dipoles. The values of typical dipole moments for the chemical species which were detected on the different surfaces of the thermoplastic fibre composites, and which affect the surface polarity, are given in table 9 (Barrow 1961; Kodokian 1990). Now, to relate the surface chemical compositions (obtained from the XPS analyses) to the values of γ_s^p (obtained from the contact angle measurements) we have defined a parameter termed the 'weighted percentage dipole moment', Ω.

To deduce the value of the weighted percentage dipole moment, Ω, for a given fibre-composite substrate, treated to a given corona intensity, several steps are involved. First, the results from the XPS analysis have been used to obtain the percentages of the chemical groups present on the surface of interest. For example, typical data for the carbon–oxygen species are given for the woven carbon-fibre/PI composite in table 5. These data have been obtained by deconvolution of the C1s peak. (Obviously, therefore, to deduce the concentration of these C–O, C═O and

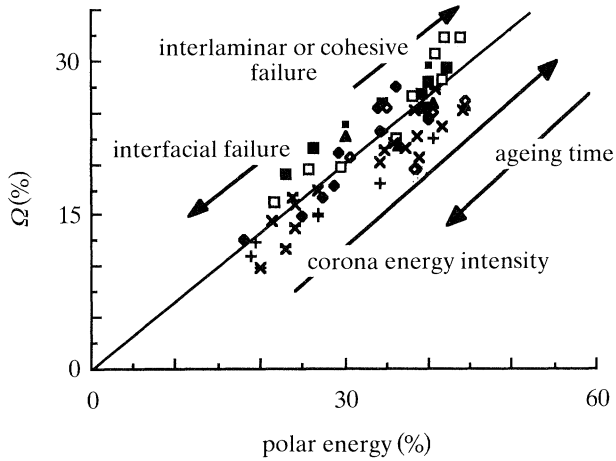

Figure 7. The value of the weighted percentage dipole mean, Ω, against percentage polar energy level for various thermoplastic fibre-composites showing the effects of using different intensities of corona treatment and aging the treated composites, before bonding. ◆, u-carbon/PEEK; ■, u-carbon/PA; □, u-Kevlar/PEEK; ×, w-carbon/PEI; +, w-carbon/PI; ∗, u-carbon/PPS; ▲, u-carbon/epoxy; ◇, u-carbon/PEEK aged; ■, u-carbon/PA aged.

O–C═O species relative to all other groups on the composite surface these concentrations of the carbon–oxygen species given in table 5 have to be multiplied by the atomic percentage of the parent C1s peak.) Also, other chemical species were usually detected, and were therefore included in the calculation of the value of Ω. For example, XPS analysis of the unidirectional carbon-fibre/PPS thermoplastic composite revealed the presence of the S═O species after the composite had been subjected to corona treatment. Secondly, the percentage values for each chemical group were then multiplied by their respective dipole moment, shown in table 9. (However, it should be noted that we did not consider the C–H species in this particular step in the calculation, since this group will only contribute to the dispersion force component, γ_s^d.) Thirdly, having obtained the individual percentage dipole moments for the different chemical species found to be present on the surface of interest, these values were then summed and normalized by 1 Debye to give the value of the weighted percentage dipole moment, Ω.

In figure 7 the value of Ω is plotted against the polar surface force component, expressed as a percentage polar surface energy, i.e. $100\,\gamma_s^p/\gamma_s$, for all the different thermoplastic fibre composites which have been subjected to various levels of corona treatment. Also, shown on this plot is a thermosetting epoxy-based carbon-fibre composite which was used as a control, and which only required a light abrasion treatment to obtain the maximum values of G_c. Although error bands are not shown on this graph, the typical scatter associated with a value of Ω for a given composite subjected to a given treatment was deduced. The scatter largely arises from that associated with the concentrations of the various chemical groups, which were measured using XPS analysis. The values of Ω quoted in figure 7 exhibit a scatter ranging from a lower bound of about $\pm 10\,\%$ to an upper bound of about $\pm 15\,\%$. As may be seen, there is a good general correlation between the value of Ω and percentage polar surface energy and, as expected, both values increase as the intensity of the corona surface treatment increases. Further, there is a critical value

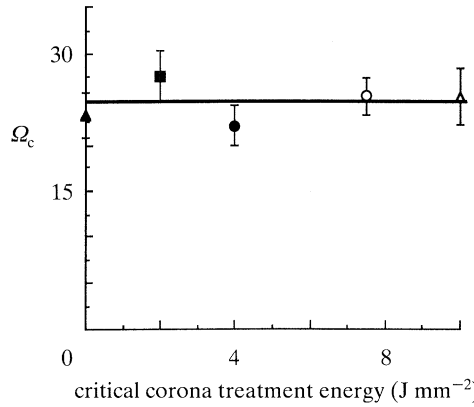

Figure 8. Critical value of the weighted percentage dipole mean, Ω_c, plotted against the intensity of the critical corona energy. In both cases the critical levels represent that needed to attain the maximum plateau value, G_c (plateau), when failure of the joint occurs cohesively through the adhesive layer. Adhesive: hot-cured epoxy. △, u-carbon/PEEK; ■, u-carbon/PA; ○, w-carbon/PEI; ●, w-carbon/PI; ▲, u-carbon/epoxy.

of either parameter which must be achieved before interfacial failure is prevented and failure of the joint occurs via fracture through the adhesive, or via interlaminar fracture of the composite. For all these fibre composites the criterion for avoiding interfacial failure, and thereby obtaining high values of the adhesive fracture energy, G_c (plateau), may be expressed by the need to attain a value of Ω of about 20 to 30% or a percentage polar energy value of about 30 to 40%. However, the precise values for these parameters will depend upon the type of adhesive used and the locus of failure which occurs when the value G_c (plateau) is attained, as discussed below.

This criterion can be more clearly seen from the data shown in figure 8. In this figure the critical value of the weighted percentage dipole moment, Ω_c, which is needed to achieve the plateau value of the adhesive fracture energy, is shown as a function of the critical corona treatment energy which is needed to attain this goal. These data were obtained using a range of fibre composites, bonded using the hot-cured epoxy adhesive, where joint failure occurred through the adhesive layer. Several interesting points arise from figure 8. First, the data confirms the earlier observations which were drawn from figure 6, namely that the critical intensity of corona treatment needed depends upon the fibre composite being used. Secondly, however, the value of Ω_c is independent of the composite being bonded, and has a value of about 25%. Indeed, a value of Ω_c of 25% leads to the prediction that no corona treatment is required for the thermosetting epoxy composite to attain a joint strength corresponding to the value of G_c (plateau); this is in complete agreement with the experimental observations. Thirdly, from figure 7, there is an equivalent critical value of the percentage polar energy, and this is about 37% for these joints.

The critical value, Ω_c, needed will be somewhat higher if a tougher adhesive is used and cohesive failure in the adhesive layer is still observed, when obviously a higher value of G_c (plateau) is recorded. For example, from the data shown in figure 6*a* and *b*, if the tougher cold-cured epoxy adhesive is used then the plateau value of G_c is about 3.9 kJ m^{-2}, compared with 1.8 kJ m^{-2} when the hot-cured adhesive is used. The tougher adhesive will obviously require higher stresses to be sustained by the

interface at failure. Hence, a higher degree of intrinsic adhesion must be attained, and a higher value of Ω_c for the composite substrates of about 28% is needed when the tougher two-part epoxy-paste adhesive is used. To achieve this higher value of Ω_c, a higher critical intensity of corona treatment is required before bonding for the composite substrate, as may be seen from figures 6*a* and 6*b*.

6.5. *The effects of ageing the corona-treated thermoplastic fibre composites before bonding*

The effects of storing, i.e. ageing, the corona-treated fibre composites before adhesive bonding may be readily understood from the above arguments. For example, if the corona-treated thermoplastic fibre composite is exposed to ambient laboratory conditions before bonding then the measured value of G_c is, in some cases, found to decrease. This is accompanied by the joint now exhibiting some degree of interfacial failure. These observations arise from the corona-treated surface of the composite adsorbing and reacting with air-borne contamination, and hence the treated surface of the thermoplastic fibre composite becomes less polar in nature. Thus, the values of Ω and the percentage polar energy for the composite surface would be expected to decrease with ageing time, and this is indeed found to occur, as shown in figure 7. Now, from the preceding discussions, once the value of Ω of the treated composite has fallen upon ageing to a value below the critical value, Ω_c, (for example, below about 25% if the hot-cured adhesive is to be used with the thermoplastic fibre composites indicated in figure 8) then it would be expected that (i) the value of G_c (plateau) would decrease, and (ii) that this would be accompanied joint failure now occurring at the adhesive/composite interface. These trends are found to be in agreement with the experimental results.

For example, for the corona-treated unidirectional carbon/PA thermoplastic composite (using a corona energy of 6 J mm^{-2}), the value of Ω had fallen to 25% after about 10 weeks of aging at ambient laboratory conditions. This value may be compared with the critical value, Ω_c, of 28%, which is needed for the composite surface to avoid interfacial failure when using the cold-cured adhesive. Experimentally, it was found that joints which were prepared after the treated composite substrates had been aged for 10 weeks, and using the cold-cured adhesive, showed a significant reduction in the value of G_c (plateau) from 3.9 kJ m^{-2} to 3.2 kJ m^{-2}. Further, a significant degree of interfacial failure was now observed. However, when using the hot-cured adhesive, where for this less tough adhesive the critical value is only 25%, then no effect of ageing the treated thermoplastic fibre-composite before bonding was observed. Thus, the effects of storing the treated composite substrates before bonding may be readily understood and quantitatively explained and, in particular, it is evident why ageing effects are often only observed when using certain types of adhesive.

7. Conclusions

The adhesive bonding of thermoplastic fibre composites, using epoxy-based structural adhesives, can be achieved if a corona treatment is used for the composite substrates before bonding. For the corona-pretreated thermoplastic composite joints the value of the adhesive fracture energy, G_c, increases steadily as the intensity of the corona treatment is increased until a maximum, plateau value of G_c is reached.

There is no evidence that any type of weak boundary layer plays a role in the

PHILOSOPHICAL TRANSACTIONS OF THE ROYAL SOCIETY A MATHEMATICAL, PHYSICAL & ENGINEERING SCIENCES

failure of the thermoplastic fibre-composite/adhesive joints. Nor is there any evidence that the degree of surface roughness induced by the corona treatment has any major effect on the intrinsic adhesion at the adhesive/composite interface. However, it has been shown that such a treatment leads to an increase in the surface concentration of polar groups, such as oxygen-containing groups, and that this leads to an increase in the surface free energy of the fibre composite substrate. This will result in an increase in both the extent of wetting by the epoxy adhesive on the substrate and the intrinsic adhesion across the adhesive/composite interface. These effects will result from enhanced interfacial interactions arising from dipole-induced dipole, dipole–dipole, hydrogen bonds and acid–base forces. The enhancement in intrinsic adhesion is reflected in the locus of failure of the DCB joints no longer being at the adhesive/composite interface, and in the far higher values of G_c which are now recorded.

It has been shown that the results obtained from contact angle measurements, surface chemical analyses and joint fracture studies may be quantitatively related. This has led to the level of surface polarity needed to attain high values of G_c being defined. Hence, it is possible to determine (i) whether a given fibre-composite needs to be subjected to a surface treatment before bonding, (ii) the level of treatment which is necessary, and (iii) the effects of aging the treated fibre composite before bonding.

Finally, it is observed that the highest plateau values of the adhesive fracture energy, G_c (plateau), are recorded when the joint fails by crack growth through the adhesive layer. It is noteworthy that under such conditions the value of G_c (plateau) may be far higher than the interlaminar fracture energy, G_c(il), of the composite material. However, in some cases, before joint failure via crack growth through the adhesive can occur, the thermoplastic composite substrate delaminates. Thus, the composite is now the 'weakest link' in the joint and the measured value of G_c (plateau) is now approximately equal in value to the interlaminar fracture energy of the composite material. Nevertheless, the propensity for the composite to delaminate in the bonded joint is not governed by the value of the interlaminar fracture energy of the composite. Instead, it is controlled by a crack initiation mechanism and is governed by the value of the out-of-plane transverse tensile fracture stress, σ_{yyc}, of the composite relative to the transverse stresses, σ_{yy}, generated in the composite substrate during loading of the joint. The transverse stresses generated in the composite substrates, in the vicinity of the crack tip in the adhesive layer, have been calculated using a finite element analysis approach and, from a comparison of the relative values of σ_{yyc} and σ_{yy}, the locus of failure observed in the various adhesively-bonded composite joints may be understood and accurately predicted. This emphasizes the importance of not only selecting the appropriate type and level of surface treatment to use for the fibre composites before bonding, but also the very significant influence that the properties of the composite substrate may have the measured performance of the bonded composite joint.

The authors are pleased to acknowledge the support and sponsorship of this work by the US Government through its European Research Office of the US Army.

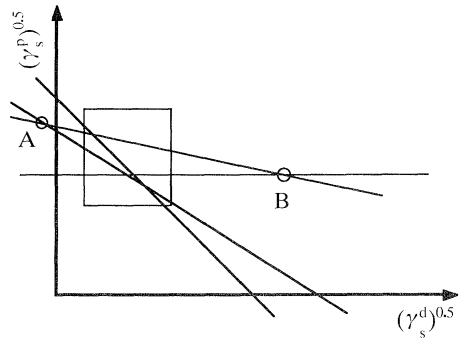

Figure 9. Schematic representation of typical individual relationships of $(\gamma_s^p)^{0.5}$ against $(\gamma_s^d)^{0.5}$ deduced from one of the simultaneous equations (see equation (3)); results from using four liquids are shown.

Appendix A. Analysis of contact angle data

Consider the schematic representation of $(\gamma_s^p)^{0.5}$ against $(\gamma_s^d)^{0.5}$ shown in figure 9, where for example, the four linear relations, obtained from using four liquids, are plotted using one of the simultaneous equations given in equation (3). Previously reported work has solved for the two unknowns using one of the following techniques.

(*a*) By solving for each individual pair of lines and then averaging the results, although this direct approach was found to lead to considerable scatter in the values of γ_s^d and γ_s^p that were obtained.

(*b*) As above, but ignoring results which are negative, e.g. point A, and values which are not close to the majority of intersections such as point B. Kaelble (1970) examined the boundaries of the rectangle shown in figure 9 and suggested that the pairs of lines which have a value of $D > 10$ mJ m^{-2} should be ignored, where D is given by equation (4). The condition that $D > 10$ mJ m^{-2} was relatively successful at reducing the scatter, but it is an arbitrary condition.

The new method proposed below for analysing the contact angle data makes it possible not only to assess the surface energy values by accepting all the experimental data, but also to obtain the least error when performing the calculations. This technique, known as the least squares method, does not depend on the individual intersections but instead on the slopes of the straight lines shown schematically in figure 9.

Now consider m equations with two unknowns in matrix form:

$$[A]_{m\times 2}[X]_{2\times 1} = [B]_{m\times 1} + [e]_{m\times 1}, \tag{A 1}$$

where matrix A represents the constant coefficients of the two unknowns in matrix X, matrix B is the constant values of the equations and matrix e is the error involved in balancing the individual equations. Now, if matrix B is taken to the left-hand side of the above equation, then

$$\{[A]_{m\times 2}[X]_{2\times 1} - [B]_{m\times 1}\} = [e]_{m\times 1}. \tag{A 2}$$

Multiplying both sides of the equality with the transpose of the left-hand side then

$$\{[A]_{m\times 2}[X]_{2\times 1} - [B]_{m\times 1}\}^{\mathrm{T}}\{[A]_{m\times 2}[X]_{2\times 1} - [B]_{m\times 1}\} = [E]_{1\times 1} \tag{A 3}$$

Table 10. *Comparison of the various methods for estimating surface free energies from contact angle data*

(All values of surface free energies in mJ m^{-2}. Condition that $D > 10$ mJ m^{-2} was used in equation (4).)

	all angles used in (3)		Kaelble method: (3) and (4)		new method (A 7)	
material	γ_s^d	γ_s^p	γ_s^d	γ_s^p	γ_s^d	γ_s^p
FEPA etched: 10 s	38.0 ± 16.8	5.9 ± 6.5	35.4 ± 8.4	5.3 ± 4.3	40.0 ± 2.6	3.2 ± 0.7
FEPA etched: 60 s	39.8 ± 46.0	14.3 ± 22.0	33.8 ± 13.7	13.4 ± 10.2	39.7 ± 4.6	6.1 ± 4.6
FEPA etched: 120 s	34.9 ± 37.7	24.8 ± 27.5	34.4 ± 13.3	15.9 ± 13.4	37.8 ± 5.4	9.7 ± 2.9
FEPA etched: 1000 s	29.2 ± 17.6	28.0 ± 26.1	35.5 ± 12.7	15.1 ± 12.3	38.5 ± 5.2	9.4 ± 2.8

and expanding the above equation gives

$$\{[X]^T[A]^T[A][X]\}_{1\times1} - \{[X]^T[A]^T[B]\}_{1\times1} - \{[B]^T[A][X]\}_{1\times1} + \{[B]^T[B]\}_{1\times1} = [E]_{1\times1}. \tag{A 4}$$

When the partial derivative of matrix E is taken with respect to the two unknowns (X_1 and X_2) and equated to zero to minimize the error then

$$\partial[E]/\partial X_1 = [A]^T[A][X] + [X]^T[A]^T[A] - [A]^T[B] - [B]^T[A] = 0$$

and

$$\partial[E]/\partial X_2 = [A]^T[A][X] + [X]^T[A]^T[A] - [A]^T[B] - [B]^T[A] = 0. \tag{A 5}$$

Since the above two equations are the same, then rearranging one of them gives

$$\{[A]^T[A][X] - [A]^T[B]\}_{2\times1} + \{[X]^T[A]^T[A] - [B]^T[A]\}_{1\times2} = 0. \tag{A 6}$$

However, the above equation is in the form of $[Z] + [Z]^T = 0$. Therefore, to satisfy the equality to zero then both matrix $[Z]_{2\times1}$ and its transpose $[A]^T{}_{1\times2}$ should be individually equal to zero, therefore

$$\{[A]^T[A][X]\}_{2\times1} = \{[A]^T[B]\}_{2\times1} \tag{A 7}$$

and

$$\{[X]^T[A]^T[A]\}_{1\times2} = \{[B]\}^T[A]\}_{1\times2}. \tag{A 8}$$

Equation (A 7) is the transpose of equation (A 8) and, therefore, only one of these two equations is required for analysis of the contact angle measurements. The benefits of this analysis are: (i) all the constant coefficients are known; (ii) it will give the minimum error; (iii) it will accept all the data and (iv) it is very simple to use.

To illustrate the differences between the different methods for analysing the same contact angle data, table 10 shows the results from contact angle data obtained by Andrews & Kinloch (1973). They examined a fluorinated ethylene–propylene copolymer (Du Pont 'FEPA') which had been chemically etched in a proprietary organic dispersion of sodium naphthalene for varying periods of time. From the results shown in table 10 it is obvious that, as reported by Kaelble (1970), the use of the simultaneous equations (equation (3)) to analyse the results from the various pairs of liquids together with equation (4) (which leads to excluding certain liquid pairs) does indeed greatly reduce the extent of scatter compared with simply using equation (3); i.e. compared with where all the various liquid pairs are included.

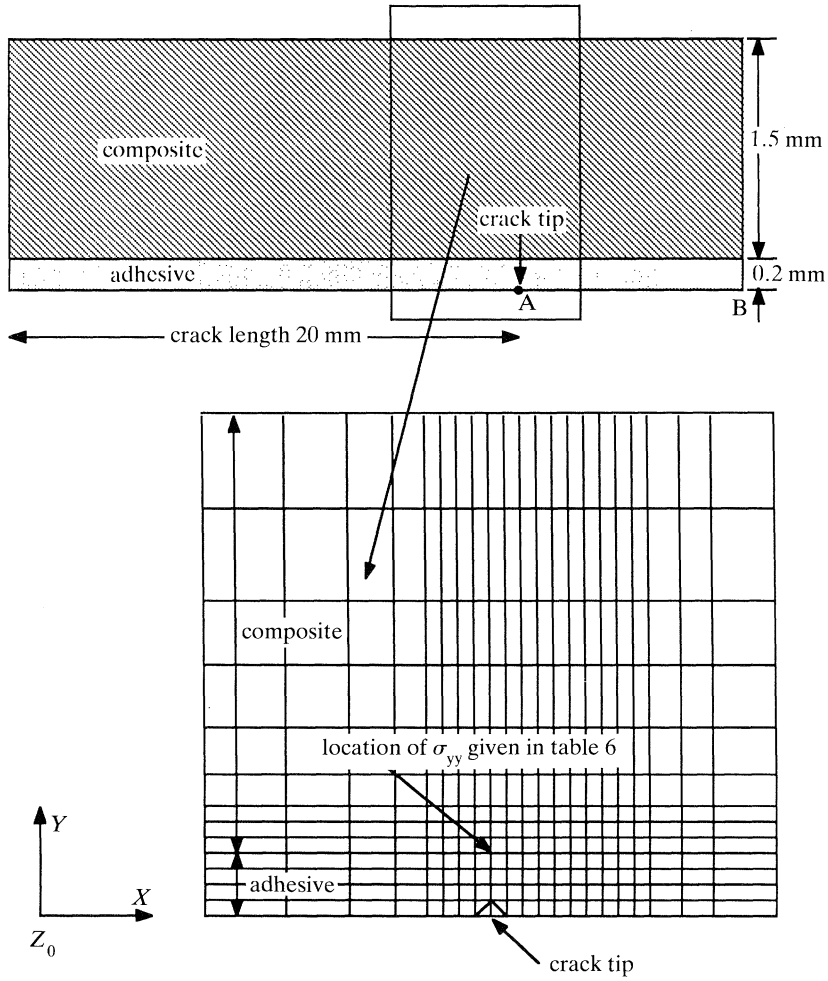

Figure 10. The finite element model of the DCB adhesive joint specimen. The upper half of the joint is illustrated. The lower diagram is an expansion of the rectangle outlined in the upper diagram and shows details of the mesh refinements around the crack tip. The scale of the lower diagram is indicated by noting that for the cold-cured epoxy adhesive the thickness of the adhesive half-layer in the model was 0.2 mm and for this case four layers of elements were used. (Whereas, for the hot-cured epoxy adhesive the thickness of the adhesive half-layer in the model was 0.25 mm and for this case five layers of elements were used.)

However, the new method, which uses equation (A 7), has the obvious advantages of using all the data and giving even lower scatter. It is suggested that the new method outlined above for analysing the contact angle data to obtain values of the dispersion, γ_s^d, and the polar, γ_s^p, force components to the surface free energy of the solid surface appears to offer considerable benefits in this area of adhesion science.

Appendix B. Finite element analysis studies

To ascertain the values of the out-of-plane transverse tensile stresses, σ_{yy}, in the vicinity of the crack tip a numerical finite element analysis (FEA) approach was

Table 11. *Material property data used in the* FEA *studies*

((*a*) Data for adhesives measured using tensile dumbell specimens; at 20 °C and at a crosshead displacement-rate of 1 mm min^{-1}. (*b*) Data for composites from manufactures (all values in 10^{-12} m^2 N^{-1}).)

(*a*) adhesive properties

material	tensile modulus/GPa	Poisson's ratio
cold-cured epoxy adhesive	1.85	0.35
hot-cured epoxy film adhesive	2.45	0.35

(*b*) composite compliance properties

material	S_{xx}	S_{yy}	S_{zz}	S_{xy}	S_{yz}	S_{zx}	SH_{xy}	SH_{zx}	SH_{yz}
u-carbon/epoxy	6.67	105	105	−1.73	−31.5	−1.73	200	200	273
u-carbon/PEEK	7.41	97.1	97.1	−2.15	−29.1	−2.15	208	208	252
u-carbon/PA	8.0	105	105	−2.32	−31.6	−2.32	200	200	273
w-Kevlar/PA	13.7	105	13.7	−3.97	−3.97	−0.82	200	200	200
u-Kevlar/PA	13.1	178	178	−4.41	−53.6	−4.41	476	476	463
w-Kevlar/PA	26.7	178	26.7	−8.0	−8.0	−2.94	145	145	145
u-carbon/PI	9.1	105	105	−2.7	−31.5	−2.7	200	200	273
w-carbon/PI	17.5	105	17.5	−5.26	−5.26	−1.4	200	200	200
u-carbon/PPS	8.13	105	105	−2.44	−31.5	−2.44	200	200	273

adopted. This consisted of using the PAFEC (1984) FEA package. For the FEA analysis a DCB joint specimen was directly drawn onto a Sigmax 6164 terminal using a multicolour two-dimensional package. The terminal was connected to a VAX computer on which the PAFEC FEA input files were run. Because of the mid-plane symmetry, only the upper half of the DCB specimen was modelled in the finite element analysis. The experimental situation was simulated on the computer such that the top left-hand node of the specimen was point loaded in small load increments to avoid sudden deflections, and hence errors. This is illustrated in figure 10. This same node was also constrained from moving in the x direction. The nodes between the crack tip (point A) and the bottom right hand node (point B) were constrained from moving in the y direction. The crack length, a, was 20 mm. Eight-noded isoparametric-curvilinear-quadrilateral elements were used throughout the specimen, except at the crack tip where four six-noded quarter-point triangular elements were used to model the singularity of the stresses at the crack tip. The elements were refined near the crack-tip region, where high-stress variations and concentrations were expected. Throughout the analysis 964 elements and 3070 nodes and 1038 elements and 3296 nodes were used for the DCB specimens bonded with the cold-cured epoxy adhesive (having a total adhesive layer thickness of 0.4 mm) and the hot-cured epoxy adhesive (having a total adhesive thickness of 0.5 mm) respectively. The type of elements used were orthotropic for the substrates and isotropic for the adhesives. All the FEA analyses were conducted assuming plane-strain conditions.

Several assumptions were made for the FEA analysis. First, it was assumed that the adhesives and composites behaved in an elastic manner. Secondly, the maximum loads used in the FEA analysis were calculated via equation (5), assuming that the crack was going to propagate in a cohesive manner through the adhesive.

Considering the material properties which are required, then an orthotropic analysis for the fibre-composite substrates requires the nine directional compliances to be known. These are

$$\left.\begin{array}{lll} S_{xx} = 1/E_{xx}, & S_{yy} = 1/E_{yy}, & S_{zz} = 1/E_{zz}, \\ S_{xy} = -\mu_{xy}/E_{xx}, & S_{yz} = -\mu_{yz}/E_{yy}, & S_{zx} = -\mu_{zx}/E_{zz}, \\ SH_{xy} = 1/G_{xy}, & SH_{zx} = 1/G_{zx}, & SH_{yz} = 1/G_{yz}, \end{array}\right\} \quad \text{(B 1)}$$

where S is the normal compliance, SH is the shear compliance, μ is Poisson's ratio, E is Young's modulus and G is shear modulus. It should be noted that the fibre reinforcement in the FEA analysis is always in the xz plane. as shown in figure 10. The material properties used in the FEA analyses for the adhesives and the composites are given in table 11.

References

American Society for Testing and Materials (ASTM) 1977 *Tensile properties of oriented fibre composites*, D3039.

Andrews, E. H. & Kinloch, A. J. 1973 *Proc. R. Soc. Lond.* A **332**, 385.

Barrow, G. M. 1961 In *Physical chemistry*, p. 302. New York: McGraw Hill.

Baszkin, A., Nishino, M. & Ter-Minassian-Saraga, L. 1977 *J. Colloid Interface Sci.* **59**, 516.

Bikerman, J. J. 1968 In *The science of adhesive joints*. New York: Academic Press.

Briggs, D., Brewis, D. M. & Konieczo, M. B. 1976 *J. mater. Sci.* **11**, 1270.

Cave, N. G., Cayless, R. A., Hazell, L. B. & Kinloch, A. J. 1990 *Langmuir* **6**, 529.

Dann, J. R. 1970 *J. Colloid Interface Sci.* **32**, 302.

Fowkes, F. M. 1967 In *Treatise of adhesion and adhesives* (ed. R. L. Patrick), p. 235. New York: Marcel Dekker.

Good, R. J. 1977 *J. Colloid Interface Sci.* **59**, 398.

Irwin, G. R. 1973 *Appl. Mater. Res.* **3**, 65.

Kaelble, D. H. 1970 *J. Adhesion* **2**, 66.

Kinloch, A. J. 1987 In *Adhesion and adhesives: science and technology*. London: Chapman and Hall.

Kinloch, A. J. & Kodokian, G. K. A. 1988 *J. Mater. Sci. Lett.* **7**, 625.

Kinloch, A. J. & Taig, C. M. 1987 *J. Adhesion* **21**, 291.

Kinloch, A. J. & Yuen, M. L. 1989 *J. mater. Sci.* **24**, 2183.

Kodokian, G. K. A. 1990 Ph.D. thesis, University of London, U.K.

Kodokian, G. K. A. & Kinloch, A. J. 1989 *J. Adhesion* **29**, 193.

Leach, D. C., Curtis, D. C. & Tamblin, D. R. 1987 ASTM STP 937, 358.

PAFEC 1984 In *PAFEC theory and user manual*. Nottingham: Strelly Hall.

Schultz, J., Tsutsumi, K. & Donnet, J. B. 1977 *J. Colloid Interface Sci.* **59**, 277.

Wenzel, R. N. 1936 *Ind. Engng Chem.* **28**, 988.

Wu, S. 1971 *J. Polymer Sci.* C **34**, 19.

Wu, S. 1973 *J. Adhesion* **5**, 39.

Received 15 April 1991; revised 11 June 1991; accepted 23 July 1991

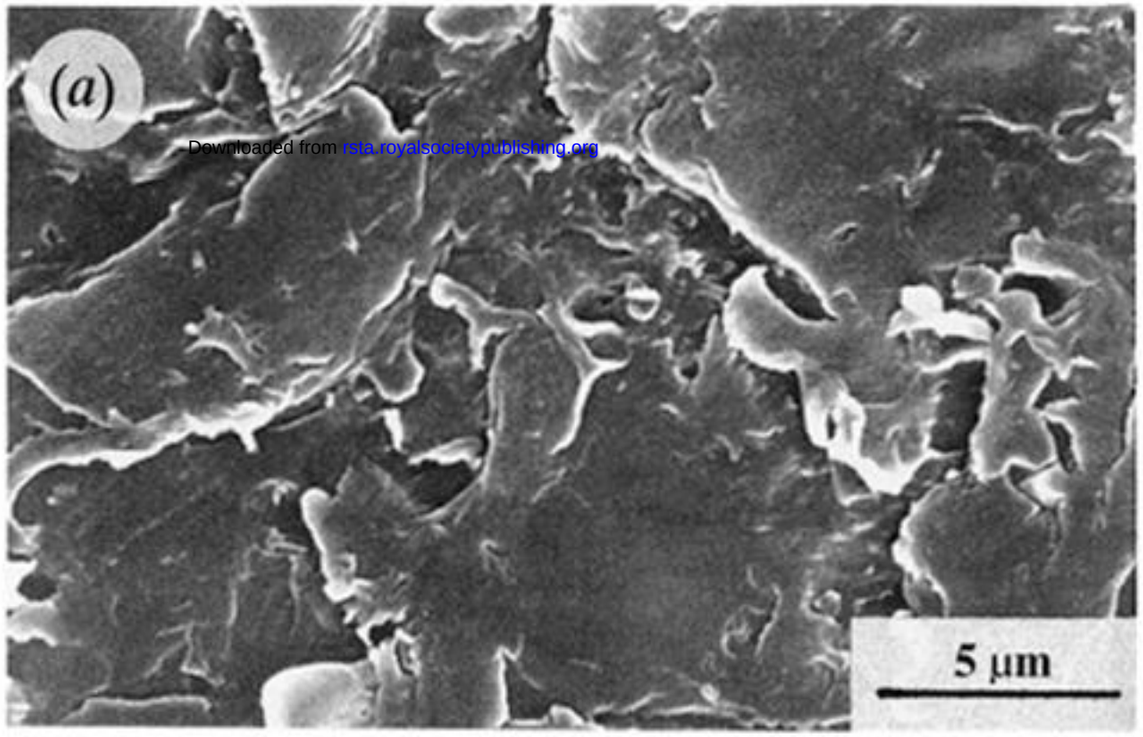

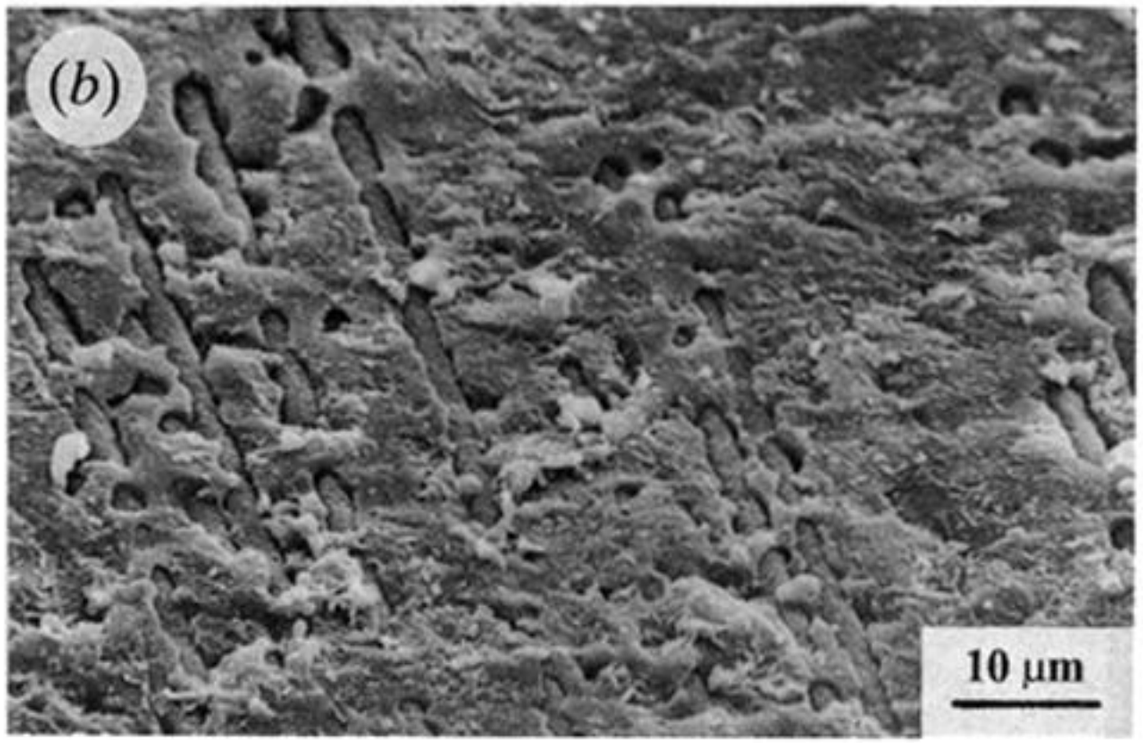

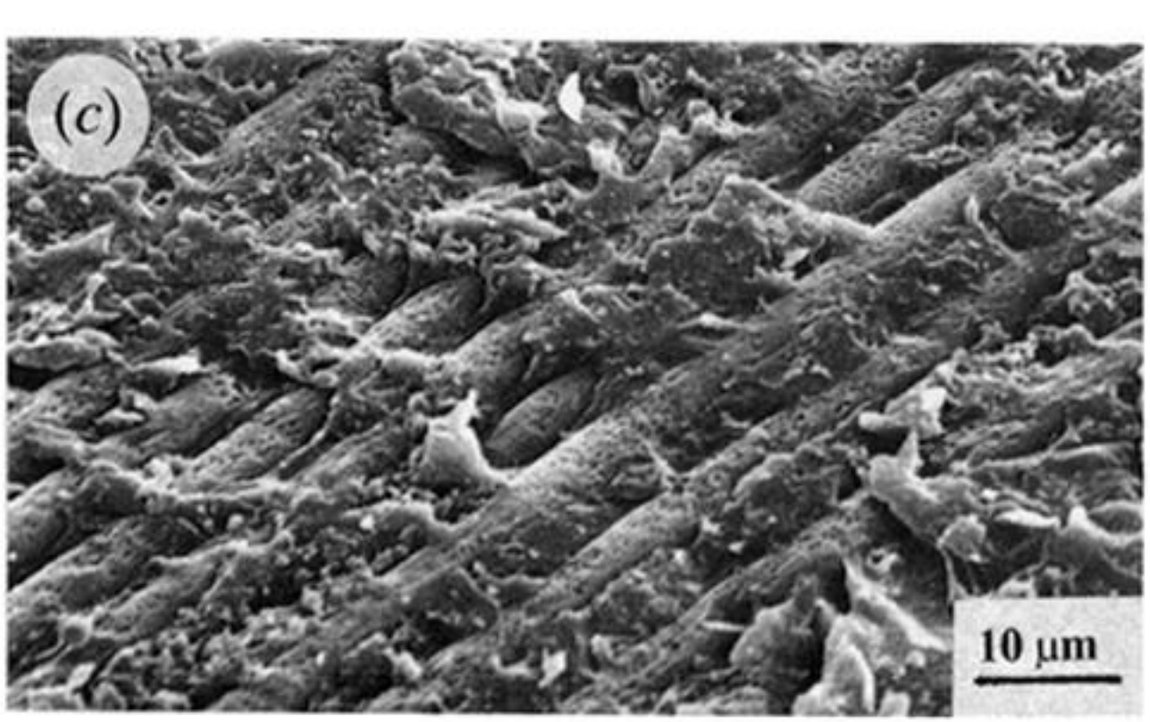

igure 1. Scanning electron micrographs of unidirectional carbon-fibre/PEEK composite subjected various treatments: (*a*) abrasion/solvent-wipe only; (*b*) corona treatment (20 J mm^{-2} of energy pplied); (*c*) corona treatment (40 J mm^{-2} of energy applied).

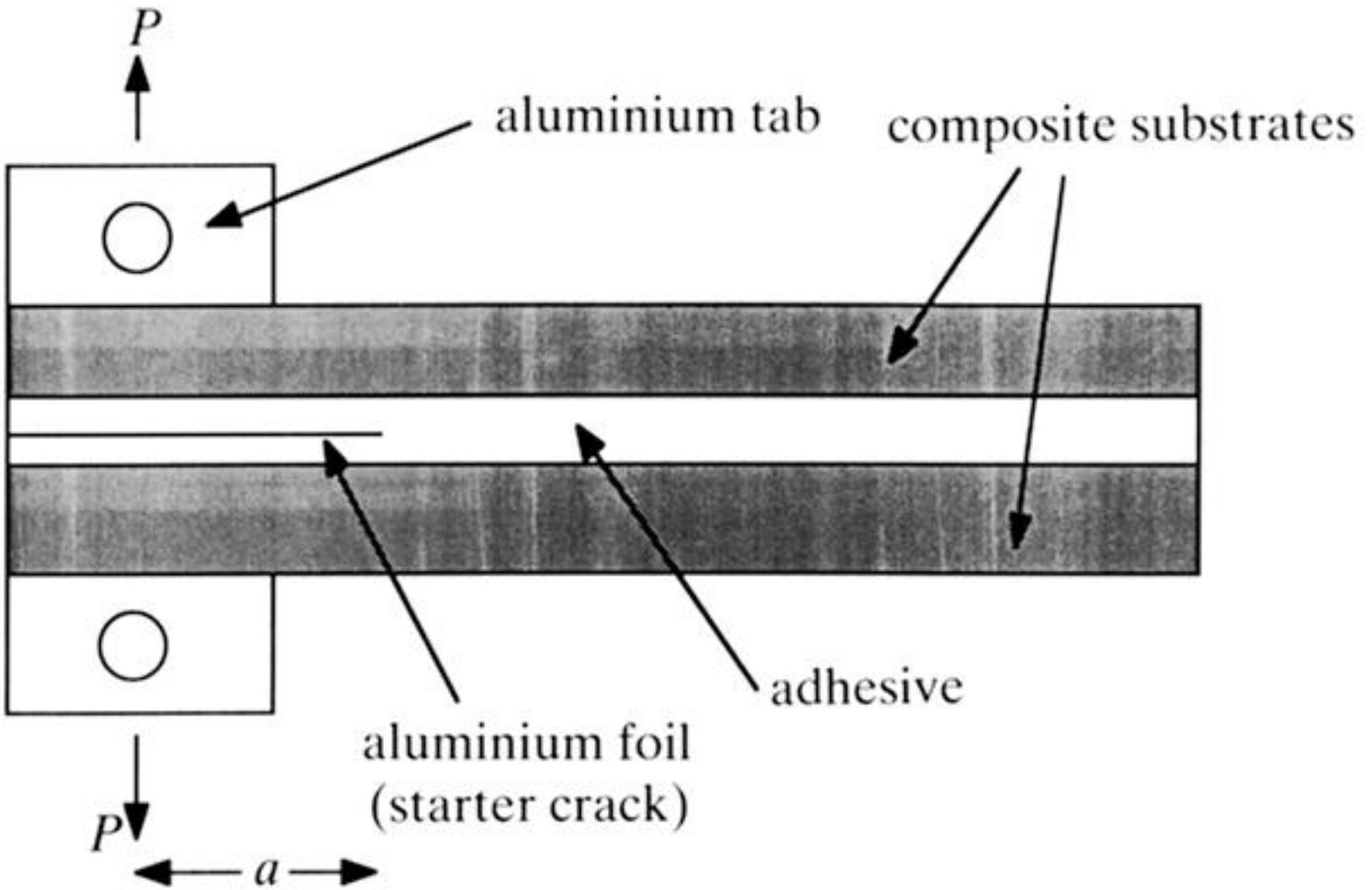

igure 5. The double-cantilever beam (DCB) joint specimen.